# Poroelastic Response of a Fractured Rock to Hydrostatic Pressure Oscillations

Samuel Chapman, Simón Lissa, Jerome Fortin, Beatriz Quintal

Geophysical Research Letters

RESEARCH LETTER
10.1029/2024GL109992

# Poroelastic Response of a Fractured Rock to Hydrostatic Pressure Oscillations

**Samuel Chapman**[1], **Simón Lissa**[2,3], **Jerome Fortin**[1], **and Beatriz Quintal**[4]

[1]Laboratoire de Géologie, Ecole Normale Supérieure/CNRS UMR 8538, PSL Research University, Paris, France, [2]FCAGLP, National University of La Plata, La Plata, Argentina, [3]CONICET, La Plata, Argentina, [4]Institute of Earth Sciences, University of Lausanne, Lausanne, Switzerland

**Key Points:**

- We observe the poroelastic coupling of fractures to the rock matrix in in-situ fluid pressure measurements during stress oscillations
- The geometrically complex fractures can be modeled as compliant and planar poroelastic inclusions
- The numerically quantified intrinsic seismic (<100 Hz) attenuation is due to fluid pressure diffusion, which is experimentally observed

**Supporting Information:**

Supporting Information may be found in the online version of this article.

**Correspondence to:**

S. Chapman,
chapman@geologie.ens.fr

**Citation:**

Chapman, S., Lissa, S., Fortin, J., & Quintal, B. (2024). Poroelastic response of a fractured rock to hydrostatic pressure oscillations. *Geophysical Research Letters*, *51*, e2024GL109992. https://doi.org/10.1029/2024GL109992

Received 25 APR 2024
Accepted 23 SEP 2024

**Abstract** Poroelastic coupling between fractures and the surrounding rock is important to numerous applications in geosciences. We measure the in-situ fluid pressure and local strain response of a fractured carbonate sample to hydrostatic pressure oscillations. A linear poroelastic model that represents the rock sample is parameterized using X-ray imaging and ultrasonic wave transmission measurements. The numerical solution, based on Biot's quasistatic equations, is consistent with the measured frequency dependent dispersion of the apparent bulk modulus of the background matrix and the in-situ pore pressure response, which is caused by fluid pressure diffusion from the compliant fractures into the stiffer matrix. The observed fluid pressure diffusion is causally related to the numerically quantified intrinsic attenuation at seismic frequencies, which is a major contributor to the dissipation of seismic waves. Our analysis supports the use of a simple approximation of fractures as compliant and planar inclusions in numerical simulations based on linear poroelasticity.

**Plain Language Summary** Fractures control the flow of fluids through rocks as well as their mechanical properties. Finding ways to accurately simulate coupled hydro-mechanical processes in fractured rock is important to a variety of applications in geosciences (e.g., subsurface storage of carbon dioxide or enhanced geothermal energy extraction). Physics-based simulations require accurate parameterization and validation against experiments. In our experiment on a fluid saturated fractured rock sample, we applied an oscillating confining pressure to the sample and measured the corresponding deformation and the change in the pore fluid pressure in a fracture and the porous matrix. By adjusting the frequency of the oscillations, we observed a divergence in the pore pressure amplitude in the fracture and the matrix, which is a consequence of flow from the fracture into the porous matrix becoming restricted at elevated frequencies. The laboratory measurements were in close agreement with the results of our simulations, which were based on a simplified model of the rock sample. The outcome of our work supports the use of a widely applied approximation of fractures as simple planar inclusions in numerical simulations based on linear poroelasticity.

## 1. Introduction

While fractures may account for only a small portion of the total porosity, they can dominate the rock's hydraulic and mechanical properties. Poroelastic coupling between fractures and the surrounding rock is important to slip on fracture surfaces, because the rate of pore pressure increase acts as a control on the likelihood of initiating seismic rupture (Alghannam & Juanes, 2020; Passelègue et al., 2020; Rudnicki & Zhan, 2020). Seismic waves are also impacted by this poroelastic coupling, because fluid pressure diffusion from the compliant fractures to the stiff matrix can be a significant source of inelastic or intrinsic seismic wave attenuation and velocity dispersion (Brajanovski et al., 2005; Gurevich et al., 2009), which is distinct from elastic or extrinsic attenuation such as the geometric spreading or reflection and refraction of a wave's energy. Improving the modeling of fractured systems and providing validation of it with experimental observations has applications in geothermal energy production, nuclear waste disposal or for the geological storage of carbon dioxide (e.g., Viswanathan et al., 2022).

The attenuation and dispersion of seismic waves in fluid saturated fractured rock has been widely studied in the framework of linear poroelasticity (M. A. Biot, 1941, 1956, 1962). A simple way of representing fractures in linear poroelasticity is to approximate them as thin compliant porous inclusions in a stiff background matrix (e.g., Brajanovski et al., 2005; Pride & Berryman, 2003). The approach allows for studying intrinsic attenuation arising from fluid pressure diffusion between the compliant fractures and the stiff background (Brajanovski et al., 2005; Gurevich et al., 2009) as well as from pressure diffusion between interconnected fractures (Quintal et al., 2014;

Rubino et al., 2013). Caspari et al. (2019) performed an extensive comparative study, utilizing both Biot's low-frequency dynamic (M. Biot, 1956, 1962) and quasi-static (M. A. Biot, 1941) equations, to simulate seismic wave propagation in models with stochastic distributions of planar fractures to investigate the relative contributions to seismic wave attenuation from transmission losses, scattering and intrinsic energy loss due to fluid pressure diffusion. The sensitivity of these mechanisms to the hydromechanical properties of the rock makes them particularly interesting in the context of seismic data processing and monitoring in fractured reservoirs (e.g., Daley et al., 2004; Rivet et al., 2016). Lissa et al. (2019, 2021) showed theoretically that approximating fractures with complex geometries as planar porous and compliant inclusions is appropriate in poroelastic numerical simulations. Such an approach of modeling fractures reduces computational costs and simplifies meshing. However, there is limited experimental evidence to support a simplified representation of fractures in numerical simulations based on poroelasticity, in part due to the complexity involved in conducting the experiments and the difficulty of accurately parameterizing the models.

The challenge of parameterizing the numerical models lies in integrating different experimental methodologies. Fracture geometry and aperture can be investigated with X-ray computed tomography (CT), while fracture compliance can for example, be determined from wave transmission measurements (Barbosa et al., 2019; Pyrak-Nolte et al., 1990). The forced oscillation method can be used to investigate the stress-strain response of fluid saturated rocks in the seismic frequency range (0–1,000 Hz) (e.g., Subramaniyan et al., 2014). Nakagawa (2013) used this method by applying axial stress oscillations to investigate the quasi-static fracture compliance of a water saturated tensile fractured sandstone, observing dispersion in both the normal and shear fracture compliance at ambient pressure conditions. Gallagher et al. (2022) investigated the response of a saw cut fracture in a carbonate sample to hydrostatic pressure oscillations and, by measuring the strain locally on the sample surface, they observed dispersion in the apparent bulk modulus of the rock matrix. In both studies, the observed dispersion in the elastic properties was attributed to fluid pressure diffusion from the compliant fracture to the stiffer background matrix. Full characterization of the poroelastic properties of rock samples, such as the Skempton coefficient (Skempton, 1954), requires also measuring the pore pressure response under undrained conditions (e.g., Hart & Wang, 1995). In-situ pore pressure measurements during forced oscillations have been performed on partially saturated and homogenous sandstone (Tisato & Quintal, 2013), however not on fractured rocks.

We measured the pore-pressure response of a naturally fractured sample to hydrostatic pressure oscillations to characterize its poroelastic response at different frequencies. We extend the work of Gallagher et al. (2022) by implementing advanced pore pressure transducers (Brantut & Aben, 2021; Lin et al., 2024) to measure the in-situ fluid pressure, determine the fracture compliance from ultrasonic wave transmission tests and characterize the fractures with micro-X-ray CT. Our experimental results validate, at first order, the linear poroelastic numerical simulations, in which we approximate the fractures by a single planar poroelastic inclusion.

## 2. Materials and Methods

### 2.1. Sample

We us a sample of Urgonian limestone from the 'Les Antennes' outcrop (43.926,516° N, 5.502,709° E) near the town of Rustrel, in the southeast of France. Urgonian limestone has been extensively studied and is considered a close analog to carbonate reservoir rocks (Borgomano et al., 2019). The cylindrical sample (length 80 mm and diameter 40 mm) was cored from the same block as the sample studied by Gallagher et al. (2022) and contains natural fractures. We investigated the sample with micro-X-ray CT (Figures 1a–1d), which revealed a set of fractures that approximately bisect the sample along its length. The main fracture extends from the top to the lower third of the sample and is slightly inclined. Another fracture extends from the bottom of the sample upwards but does not appear connected with the main fracture. The mean aperture of the fractures, at ambient pressure, is estimated at 310 μm, the maximum aperture measured is 480 μm and the minimum aperture is below the scanning resolution of 30 μm. The fractured volume is highest toward the top of the sample (Figure 1b), where the main fracture connects to a larger void. The total porosity of the sample is 19.80 ± 0.02%, determined with the triple-weight method as well as by assuming the matrix of the sample is composed purely of calcite (e.g., Dullien, 1992). The porosity of the matrix is 18.5 ± 0.3% and was determined from the average of two subsamples. The uncertainty in the porosity measurements is estimated from the propagation of the weight measurement error of 0.01 g. The water permeability of the sample is 0.11 ± 0.03 mD, measured at an effective pressure ($P_{eff} = P_c - p_f$) of 2.5 MPa.

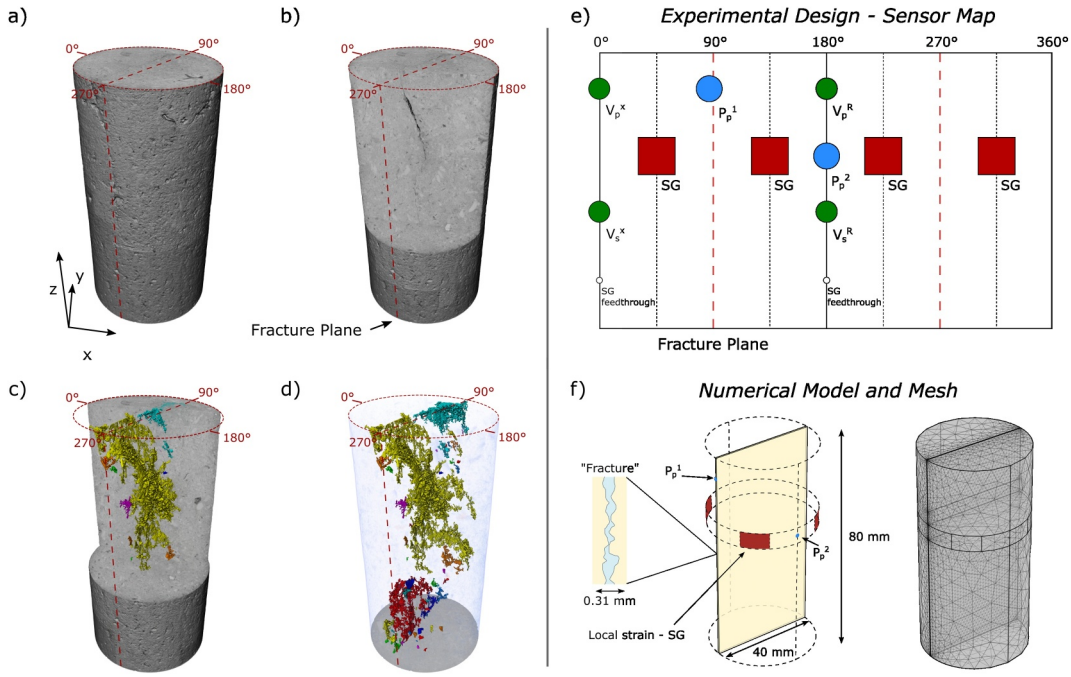


**Figure 1.** (a)-(d) Micro X-ray CT of the sample and the segmented fractures. The CT scan was coarsened to a resolution of $60 \times 60 \times 60$ µm. e) Schematic of the sensor layout on the unwrapped surface of the sample. The sensors used include: a pair of ultrasound P- and S-wave transducers ($V_p$, $V_s$), two pore pressure transducers ($P_p$) and four pairs of strain gauges (SG) in a bi-axial configuration. The approximate location of the fracture plane is indicated by the red dashed line. f) Outline of the numerical model and mesh. The volumetric strain is averaged over the small rectangular patches (red), analogous to the local strain measured during the experiments by the strain gauges.

### 2.2. Experimental Methodology

To investigate the poroelastic properties of the sample, experiments were carried out in a triaxial cell (Borgomano et al., 2020). The sensor layout is shown in Figure 1e. The deformation of the porous matrix was measured with four pairs of bi-axial strain gauges, placed at approximately 45° to the main fracture plane. The local pore pressure was measured with two pore-pressure transducers (Brantut & Aben, 2021). One transducer ($P_p^1$) was placed where the fracture intersects the surface of the sample and the other ($P_p^2$) was placed at approximately 90° to the main fracture plane, to measure the pore pressure in the porous matrix. A pair of ultrasound P- and S-wave transducers (0.5 MHz central frequency) were used to measure the wave velocities perpendicularly across the fractures.

Forced oscillations on the sample were performed by imposing sinusoidal oscillations of the confining pressure ($P_c$). Measurements were performed in the frequency range of 0.004–1 Hz and at a maximum amplitude ($\Delta P_c$) of 0.3 MPa, which induce uniaxial strains of less than $10^{-5}$, which are sufficiently low to assume the measurements are in the linear elastic regime (e.g., Chapman et al., 2023; Winkler et al., 1979). A Fourier analysis was carried out on the confining pressure, pore pressure and strain signals to determine the respective amplitudes and phases at the imposed frequencies (e.g., Batzle et al., 2006). We determine an apparent bulk modulus $K$ for the matrix from the stress and strain amplitudes:

$$K(f) = \frac{\Delta P_c\,(f)}{\Delta \varepsilon_{vol}\,(f)}, \tag{1}$$

where $\varepsilon_{vol} = \varepsilon_{ax} + 2\varepsilon_{rad}$, with $\varepsilon_{ax}$ and $\varepsilon_{rad}$ being the axial and radial strains, respectively. We refer to the bulk modulus as apparent because it is determined from the local strain measured on the background matrix and is there for not representative of the entire sample deformation.

Initial measurements were performed on the dry sample, after which the sample was saturated with glycerin. We use glycerin as a saturating fluid because of its high viscosity, which is temperature dependent, allowing us to

observe dispersive behavior in the elastic moduli of the sample at low frequencies (<1 Hz). The pore fluid pressure $p_f$ was maintained at 5 MPa during all subsequent measurements. Hydrostatic oscillations of the confining pressure were performed at effective pressures of 2.5, 5 and 7.5 MPa and temperatures of 19°C, 25°C and 45°C. All hydrostatic pressure oscillations were performed with undrained boundary conditions, by closing the hydraulically activated micro-valves in the sample holders (Borgomano et al., 2020). The viscosity of the glycerin is temperature dependent, allowing us to investigate a broader frequency range, by scaling the probing frequency with respect to the fluid viscosity. We define this apparent frequency in the following way (e.g., Jones & Nur, 1983; Vo-Thanh, 1990):

$$f_{app} = f\frac{\eta_f}{\eta_0}, \tag{2}$$

where $f$ is the frequency and $\eta_f$ and $\eta_0$ are the viscosity of the fluid and the reference viscosity, respectively. The reference viscosity is the fluid viscosity at 45°C. By applying a steady state flow through the sample, the fluid viscosity at each temperature was inverted from the fluid pressure gradients and flow rate, assuming that the permeability is the same as in the water saturated sample.

To probe the elastic properties of the sample, P- and S-waves were transmitted across or approximately normal to the fractures. These measurements were carried out on the dry sample after the initial experiments, under ambient and confining pressure (maximum confining pressure of 17.5 MPa). At ambient conditions only P-waves were transmitted, perpendicular to the fracture plane. Measurements were performed at multiple locations along the length of the sample ($z$-axis) by moving both transducers such that the travel path remained perpendicular to the fractures. For comparison, velocity measurements were also performed on an intact (non-fractured) sample that was cored from the same block.

We utilize the ambient measurements on the fractured and intact samples to determine the fracture normal compliance. The fractures are assumed to obey linear slip theory, where the displacement induced by the wave is discontinuous across the fracture, but the stress is continuous (Schoenberg, 1980). Under this assumption the normal fracture compliance $Z$ can be related to the transmission coefficient $|T(\omega)|$ as follows (Pyrak-Nolte et al., 1990):

$$Z = \frac{2}{\rho v \omega}\sqrt{\frac{1}{T^2} - 1}, \tag{3}$$

where $\rho$ is the bulk density of the intact rock, $v$ is the P-wave velocity in the intact rock and $\omega$ is the angular frequency. We determine the transmission coefficient from the time domain ratio of the peak-to-peak amplitude of the waveforms of the fractured and intact samples (Möllhoff et al., 2010). An average fracture compliance is calculated from four measurements, where the quality of the waveforms allowed for determining a peak-to-peak amplitude, giving us an effective fracture compliance. For additional details, we refer the reader to the supplementary information.

### 2.3. Numerical Simulations

The theoretical hydro-mechanical response of the fractured sample to pressure oscillations was studied by numerically solving Biot's (1941, 1962) quasi-static equations of poroelasticity. The simulations were performed with COMSOL Multiphysics, where the discretized finite element expressions of the equations (Quintal et al., 2011) were solved in the frequency domain. A cylindrical numerical model represents the laboratory sample (Figure 1f). The fracture and matrix are treated as isotropic porous materials saturated by a single fluid. The fracture network observed in the rock sample is approximated in the model as a single porous layer of 0.31 mm thickness. Such a simplified approach has been shown to be appropriate for modeling the effective poroelastic response of fractures (Lissa et al., 2019). The bulk and shear modulus of the planar fracture in the model are determined from the average normal fracture compliance derived from the ultrasound measurements. The other material properties, such as the porosity, permeability and bulk and shear moduli of the solid matrix, used for the numerical simulations, are based on direct experimental measurements, which are described in the supplementary information and summarized in Table S1 of Supporting Information S1.

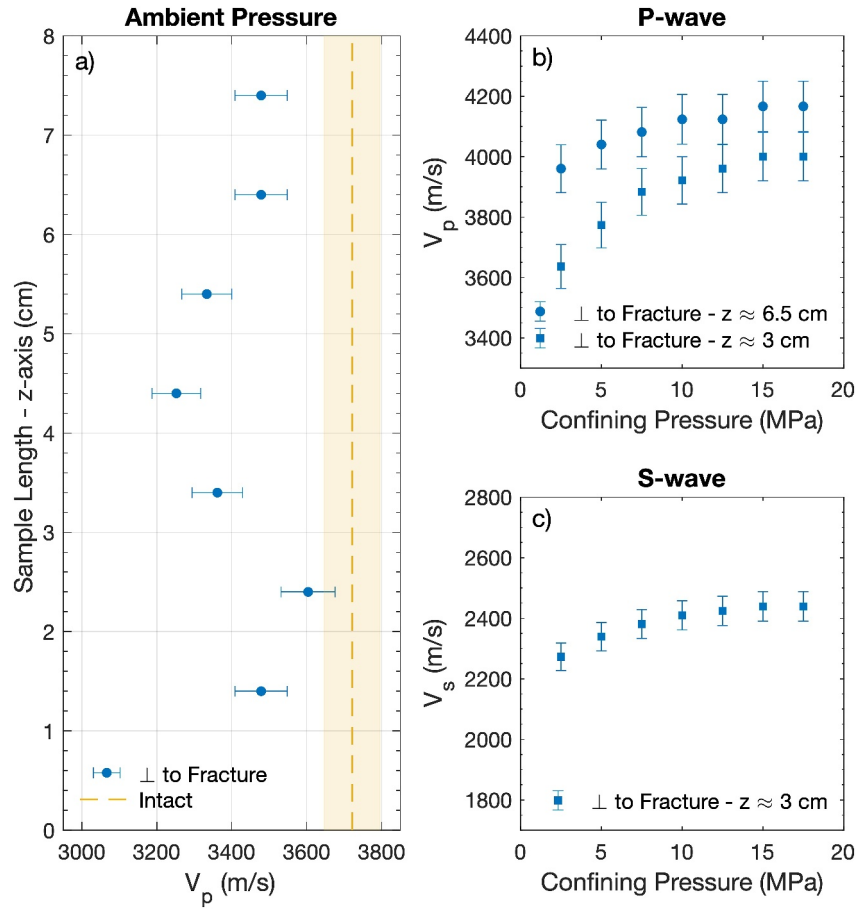


**Figure 2.** Ultrasonic wave velocities (0.5 MHz) measured on the dry sample. (a) P-wave velocity ($V_p$) measured perpendicular (⊥) to the fracture plane at ambient pressure, as a function of the position along the length of the sample ($z$-axis). The yellow dashed line indicates the P-wave velocity measured on the intact sample. (b)-(c) P-wave and S-wave velocity ($V_s$), measured perpendicular to the fracture plane, as a function of confining pressure. The uncertainties in the P-wave and S-wave velocities are estimated at ±2%.

Boundary conditions are chosen for the numerical model that are representative of the experimental conditions. At the outer model boundary, a relative fluid velocity of zero is considered in the finite element expressions (Quintal et al., 2011), corresponding to the undrained boundary condition of the laboratory experiment. The confining pressure oscillations of the experiment are simulated by applying an oscillatory displacement at the model boundaries, corresponding to a bulk volumetric compression of the model domain. In this way, we determined the frequency dependent evolution of solid displacement and fluid pressure. From the calculated stress and strain, averaged over small volumes at the model surface (Figure 1f), corresponding to the local strain measurements, we determined a local complex bulk modulus (Chapman & Quintal, 2018; Pimienta et al., 2016). From the stress and strain averaged over the whole model, we obtain the global bulk modulus and corresponding attenuation (Jänicke et al., 2015). For more details of the numerical simulations, we direct the reader to the Supporting Information S1, which includes a validation of the numerical implementation against an analytical solution.

## 3. Elastic Wave Velocity and Fracture Compliance

The heterogeneity of the elastic properties and their pressure dependence are captured well by the ultrasonic P- and S-wave velocities measured on the dry sample. At ambient pressure conditions, the P-wave velocity varies significantly along the length of the sample (Figure 2a). The velocity is lowest in the center of the sample, 300–400 m/s lower than the intact sample. The measurements at $z = 2.7$, 3.7, 5.7 and 6.7 cm were used to determine the average fracture compliance of $5.9 \times 10^{-12}$ m/Pa, with a range from $2 \times 10^{-12}$ to $1.1 \times 10^{-11}$ m/Pa. The pressure dependence of the P- and S-wave velocities, measured perpendicular to the main fracture plane, reflects the closure

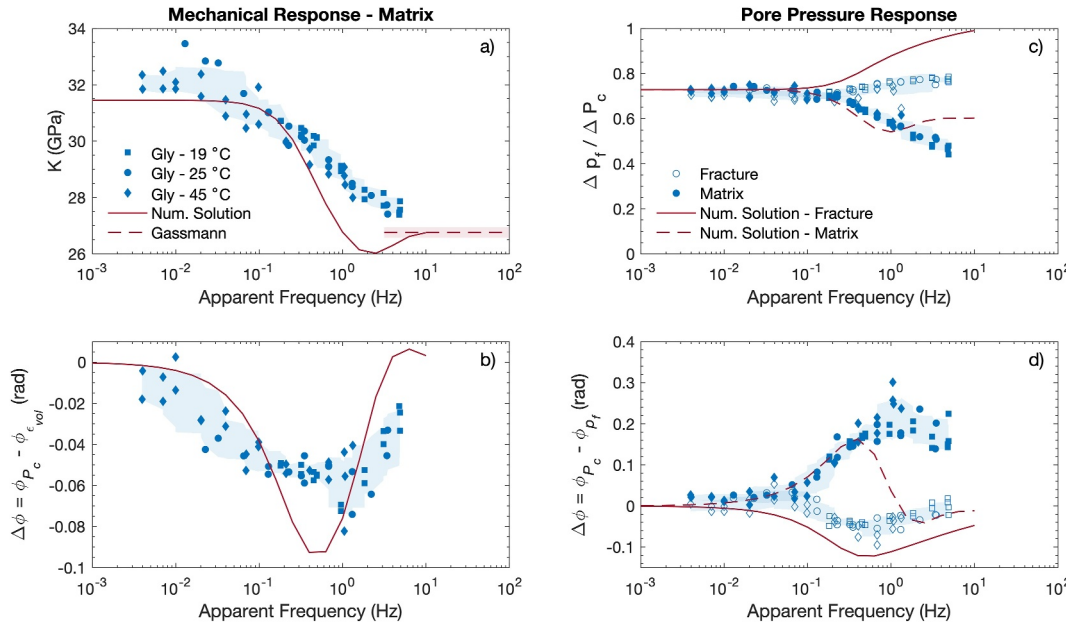


**Figure 3.** Experimental results of the hydrostatic pressure oscillations on the fluid saturated sample and the poroelastic numerical solution. (a) Apparent bulk modulus $K$ calculated from the local strain on the surface of the rock sample and the numerical model. (b) Phase difference between the confining pressure and local volumetric strain. (c) Ratio of pore pressure to confining pressure amplitude, measured by the pore pressure transducers at the fracture and the matrix. (d) Phase difference between the confining pressure and local pore pressure. Blue shaded regions indicate an estimate of the measurement uncertainty based on a moving standard deviation (window size of 10). The effective pressure during the experiments was 2.5 MPa.

of the fractures (Figures 2b and 2c). The P-wave velocity measured at $z = 6.5$ cm is significantly higher than the velocity measured in the intact sample at ambient conditions, indicating that the nonlinear pressure dependence of the wave velocities is due to the closing of not only the mesoscale fractures, but also microscale cracks and grain contacts.

## 4. Fracture to Matrix Pore-Fluid Pressure Diffusion

We measured the poroelastic response of the fluid saturated sample in response to sinusoidal oscillations of the confining pressure. For brevity we focus on the experimental results measured at 2.5 MPa effective pressure, where we observe negative dispersion in the apparent bulk modulus from 33 to 28 GPa, with increasing apparent frequency (Figure 3a). At high frequencies the bulk modulus appears to converge to the undrained limit for an ideal porous material, which was calculated with Gassmann's (1951) equation. We also observe a negative phase difference between the confining pressure and locally measured volumetric strain (Figure 3b), indicating an apparent lagging of the applied pressure behind the strain response. The induced pore pressure response is the same at the fracture and the matrix at low frequencies (Figure 3c), with a pore pressure to confining pressure ratio of $0.71 \pm 0.02$, indicating that the pore pressure throughout the sample is equilibrated. With increasing frequency, the pore pressure response at the fracture and matrix diverges. At the fracture, the ratio increases to $0.77 \pm 0.01$, while at the matrix it decreases to $0.48 \pm 0.03$. The divergence in the pore pressure response shows that fluid flow from the compliant fracture to the stiff matrix is progressively reduced with increasing frequency, that is, the time scale is too short for pressure diffusion to occur. The phase difference between the confining pressure and pore fluid pressure is positive in the matrix and negative in the fracture, for frequencies >0.1 Hz (Figure 3d).

The poroelastic response of the sample was also measured at effective pressures of 5 and 7.5 MPa. With increasing effective pressure, we observed an increase in the bulk modulus of the dry matrix and an overall reduction in the pore pressure to confining pressure ratio of the saturated sample. Dispersion with respect to frequency in the apparent bulk modulus and the corresponding phase shift between pressure and strain also decrease with increasing effective pressure. At frequencies >0.1 Hz, we again observe the divergence between the

pore pressures measured at the fracture and porous matrix. We summarize the key observations in Table S2 of Supporting Information S1.

The numerical simulation reproduces at first order the experimental observations. Indeed, there is good agreement with the measured low and high frequency limits of the bulk modulus (Figure 3a). Both the numerically calculated dispersion and phase difference show a transition over a narrower frequency band than the experimental results (Figures 3a and 3b). At low frequencies, the numerical solution reproduces well the measured pore pressure response, predicting a pore pressure to confining pressure ratio of 0.73 compared to the measured ratio of $0.71 \pm 0.02$ (Figure 3c). At high frequencies, the numerical solution overestimates the pressure response in the fracture, reaching the limit of 1. The numerical solution predicts that the pressure in the matrix decreases and then stabilizes at a ratio of 0.6. The phase difference predicted by the numerical solution is in reasonable agreement with the experimental observations (Figure 3d). For the fracture the negative phase difference is generally overestimated, while for the matrix the results diverge from the experimental observations at high frequencies, reaching a maximum at 0.5 Hz before decrease again.

## 5. Discussion

The experiments we performed on a rock sample with natural fractures are an extension and generalization of experiments performed by Gallagher et al. (2022) on a sample with a saw cut fracture. The dispersion in the apparent bulk modulus as well as the phase difference between stress and strain (Figures 3a and 3b) are consistent with the experimental observations of Gallagher et al. (2022). The numerical solution, based on poroelasticity, for our simple model captures to first order our observations. The model accurately predicts the characteristic frequency, at which the maximum phase difference occurs, as well as the high and low frequency limits of the bulk modulus dispersion. However, the numerical solution shows a sharper transition than the experimental results and, while the pore pressure response is accurately modeled at low frequencies, the measurements and numerical solution diverge at high frequencies. These discrepancies are likely due to a lack of heterogeneity in the numerical model. The fractures are approximated as a simple planar feature embedded in a homogenous background matrix, which imposes a single characteristic time over which fluid pressure diffusion occurs. The heterogeneity of the rock sample is clearly shown in the variation of the P-wave velocity along its length (Figure 2a), though it is not clear whether this is due only to variations in the fracture compliance or also includes variations in the stiffness of the background matrix. Heterogeneity in the permeability of the matrix is probably another important factor that could explain the deviations (Figure 3c), as it would introduce a range of characteristic times over which fluid pressure diffusion occurs. The subsample-scale permeability can be quite variable even in porous rocks considered to be homogeneous (Pini & Benson, 2017). We also do not account for the fact that the fractures are slightly inclined and possibly not fully connected, though we expect this to minimally impact the diffusion time from the fractures to the porous background. The overestimation in the numerical solution of the pore pressure response in the fracture may be because we use an effective fracture compliance whereas the sensor, at high frequencies, is probing a smaller portion of the fractures that is comparatively stiffer. This interpretation is supported by the X-ray CT images showing a larger void connected to the fracture at the measurement location (Figure 1b).

The approximation of fractures as compliant and fluid saturated poroelastic inclusions of simple geometries is widely used to theoretically investigate the attenuation and dispersion of seismic waves (e.g., Brajanovski et al., 2005; Gurevich et al., 2009; Quintal et al., 2014; Rubino et al., 2013). The appropriateness of such an approach has been numerically demonstrated by Lissa et al. (2019, 2021) and is supported by our experimental study. More generally, our experiments and numerical simulations provide strong evidence that the hydro-mechanical coupling of fractures to a porous background matrix can be modeled in the framework of linear poroelasticity. Furthermore, by measuring the pore pressure response at the fracture and the matrix, we directly observe fluid pressure diffusion from the compliant fractures into the porous matrix in response to frequency dependent oscillations of an externally applied stress (Figures 3c and 3d). Fluid pressure diffusion is an important source of intrinsic attenuation of seismic P- (Brajanovski et al., 2005) and S-waves (Quintal et al., 2014) in fluid saturated fracture rock.

We could not directly calculate the attenuation from the measured phase shift between stress and strain (Masson & Pride, 2014; O'Connell & Budiansky, 1978). To determine the attenuation in this way, stress and strain must be averaged over the entire domain (Jänicke et al., 2015). In our experiment this condition was not met, because we

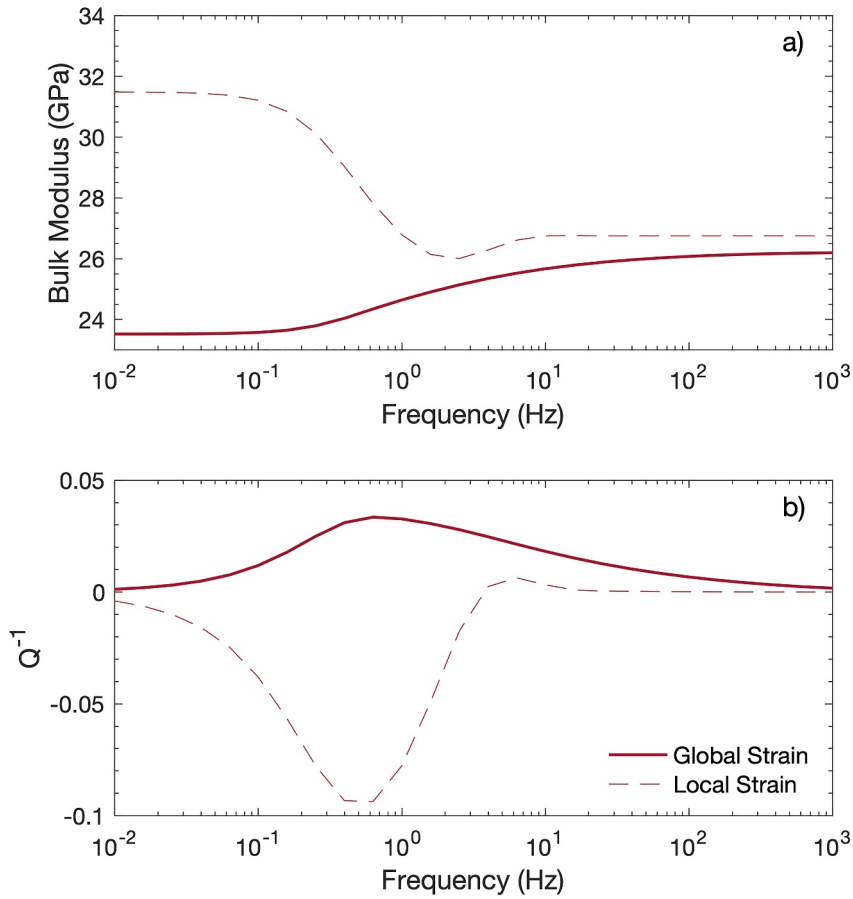


**Figure 4.** Numerical results from the poroelastic rock model of (a) bulk modulus dispersion and (b) corresponding attenuation $Q^{-1}$ determined from the global strain. The dashed lines correspond to the numerical results presented in Figures 3a and 3b, where the strain was locally averaged corresponding the location of the strain gauges in the experiment.

measured the strain locally on the surface of the sample with strain gauges and the material properties of the sample vary spatially by orders of magnitude because of the presence of the mesoscale fractures. To quantify the attenuation and dispersion associated with the observed fluid pressure diffusion we can, however, average the stress and strain from our numerical simulations over the entire model domain. Unlike when stress and strain are averaged locally (Figure 3), the globally measured bulk modulus increases from high to low frequencies (Figure 4a). The attenuation reaches a maximum at 0.63 Hz, which is at the lower end of the seismic wave frequency band (Figure 4b). In the context of a subsurface reservoir, the attenuation peak could easily occur at higher frequencies due to a lower fluid viscosity, with an increase in permeability of the background matrix or with a decrease in the spacing between fractures (Brajanovski et al., 2005). More experimental research is needed to investigate the attenuation and dispersion in fluid saturated rocks due to fluid pressure diffusion between interconnected fractures, where attenuation is expected to be significantly greater and at higher frequencies (Quintal et al., 2014; Rubino et al., 2013). Such experiments would be greatly improved by measuring the strain over the entire sample and not locally with strain gauges.

## 6. Conclusions

We investigated experimentally and numerically the poroelastic response of a fluid saturated rock sample with natural fractures to hydrostatic pressure oscillations. With advanced pressure transducers we were able to probe the in-situ pore fluid pressure of the sample at two locations, allowing us to observe the poroelastic coupling between the fractures and the porous background. We were able to observe mesoscopic fluid pressure diffusion from the compliant fractures to the stiffer porous background, which is a source of intrinsic attenuation of seismic waves. Our poroelastic numerical simulations reproduce at first order our experimental observations. Even

though the complex fractures that bisect the sample are approximated as a single compliant porous layer in our model, we accurately predict the characteristic frequency at which the phase difference between stress and strain reaches a maximum and the high and low frequency limits in the apparent bulk modulus of the matrix. Our observations and analysis provide experimental support for such a modeling approach, based on Biot's theory of linear poroelasticity, that is widely used to study seismic wave propagation in fluid saturated and fractured rock.

## Data Availability Statement

The data presented in this article are available at the following repository via Chapman et al. (2024).

**Acknowledgments**
This research was supported by the Swiss National Science Foundation (Grant 172691). We would like to thank Jörg Renner and an anonymous reviewer for their thorough review. Jörg Renner's attention to detail in particular helped to significantly improve the accuracy and clarity of the manuscript. Special thanks go to Ariel Gallagher for providing the sample, Lucas Baumgartner for helping with the micro-X-ray computed tomography, Nicolas Barbosa for helpful discussions concerning the numerical simulations and Cedric Bailly for discussions concerning possible diagenesis and mineral dissolution in the sample.

## References

Alghannam, M., & Juanes, R. (2020). Understanding rate effects in injection-induced earthquakes. *Nature Communications*, *11*(1), 3053. https://doi.org/10.1038/s41467-020-16860-y

Barbosa, N. D., Caspari, E., Rubino, J. G., Greenwood, A., Baron, L., & Holliger, K. (2019). Estimation of fracture compliance from attenuation and velocity analysis of full-waveform sonic log data. *Journal of Geophysical Research: Solid Earth*, *124*(3), 2738–2761. https://doi.org/10.1029/2018JB016507

Batzle, M. L., Han, D.-H., & Hofmann, R. (2006). Fluid mobility and frequency-dependent seismic velocity - direct measurements. *Geophysics*, *71*(1), N1–N9. https://doi.org/10.1190/1.2159053

Biot, M. A. (1941). General theory of three-dimensional consolidation. *Journal of Applied Physics*, *12*(2), 155–164. https://doi.org/10.1063/1.1712886

Biot, M. A. (1956). Theory of propagation of elastic waves in a fluid-saturated porous solid. I. Low-frequency range. *Journal of the Acoustical Society of America*, *28*(2), 168–178. https://doi.org/10.1121/1.1908239

Biot, M. A. (1962). Mechanics of deformation and acoustic propagation in porous media. *Journal of Applied Physics*, *33*(4), 1482–1498. https://doi.org/10.1063/1.1728759

Borgomano, J. V. M., Gallagher, A., Sun, C., & Fortin, J. (2020). An apparatus to measure elastic dispersion and attenuation using hydrostatic- and axial-stress oscillations under undrained conditions. *Review of Scientific Instruments*, *91*(3), 034502. https://doi.org/10.1063/1.5136329

Borgomano, J. V. M., Pimienta, L. X., Fortin, J., & Gueguen, Y. (2019). Seismic dispersion and attenuation in fluid-saturated carbonate rocks: Effect of microstructure and pressure. *Journal of Geophysical Research: Solid Earth*, *124*(12), 12498–12522. https://doi.org/10.1029/2019JB018434

Brajanovski, M., Gurevich, B., & Schoenberg, M. (2005). A model for P-wave attenuation and dispersion in a porous medium permeated by aligned fractures. *Geophysical Journal International*, *163*(1), 372–384. https://doi.org/10.1111/j.1365-246x.2005.02722.x

Brantut, N., & Aben, F. M. (2021). Fluid pressure heterogeneity during fluid flow in rocks: New laboratory measurement device and method. *Geophysical Journal International*, *225*(2), 968–983. https://doi.org/10.1093/gji/ggab019

Caspari, E., Novikov, M., Lisitsa, V., Barbosa, N. D., Quintal, B., Rubino, J. G., & Holliger, K. (2019). Attenuation mechanisms in fractured fluid-saturated porous rocks: A numerical modelling study. *Geophysical Prospecting*, *67*(4), 935–955. https://doi.org/10.1111/1365-2478.12667

Chapman, S., Fortin, J., Gallagher, A., & Borgomano, J. V. M. (2023). Strain amplitude dependent transition from dynamic to static bulk modulus in rocks with and without pre-existing cracks. *Rock Mechanics and Rock Engineering*, *56*(8), 6101–6118. https://doi.org/10.1007/s00603-023-03392-2

Chapman, S., Lissa, S., Fortin, J., & Quintal, B. (2024). Data: Poroelastic response of a fractured rock to hydrostatic pressure oscillations. *Zenodo*. [Dataset]. https://doi.org/10.5281/zenodo.11067586

Chapman, S., & Quintal, B. (2018). Numerical analysis of local strain measurements in fluid saturated rocks submitted to forced oscillations. *Geophysics*, *83*(5), MR309–MR316. https://doi.org/10.1190/geo2018-0071.1

Daley, T. M., Majer, E. L., & Peterson, J. E. (2004). Crosswell seismic imaging in a contaminated basalt aquifer. *Geophysics*, *69*(1), 16–24. https://doi.org/10.1190/1.1649371

Dullien, F. A. L. (1992). Porous media. Second Edition. In *Fluid transport and pore structure*. Academic Press, Inc. 92101.

Gallagher, A., Fortin, J., & Borgomano, J. (2022). Seismic dispersion and attenuation in fractured fluid- saturated porous rocks: An experimental study with an analytic and computational comparison. *Rock Mechanics and Rock Engineering*, *55*(7), 4423–4440. https://doi.org/10.1007/s00603-022-02875-y

Gassmann, F. (1951). Über die Elastizität poröser Medien: Vierteljahrsschrift der Naturforschenden Gesellschaft in Zürich, *96*, 1–23.

Gurevich, B., Brajanovski, M., Galvin, R. J., Müller, T. M., & Toms-Stewart, J. (2009). P-wave dispersion and attenuation in fractured and porous reservoirs – Poroelasticity approach. *Geophysical Prospecting*, *57*(2), 225–237. https://doi.org/10.1111/j.1365-2478.2009.00785.x

Hart, D. J., & Wang, H. F. (1995). Laboratory measurements of a complete set of poroelastic moduli for Berea sandstone and Indiana limestone. *Journal of Geophysical Research*, *100*(B9), 17741–17751. https://doi.org/10.1029/95JB01242

Jänicke, R., Quintal, B., & Steeb, H. (2015). Numerical homogenization of mesoscopic loss in poroelastic media. *European Journal of Mechanics - A: Solids*, *49*, 382–395. https://doi.org/10.1016/j.euromechsol.2014.08.011

Jones, T., & Nur, A. (1983). Velocity and attenuation in sandstone at elevated temperatures and pressures. *Geophysical Research Letters*, *10*(2), 140–143. https://doi.org/10.1029/gl010i002p00140

Lin, G., Chapman, S., Garagash, D. I., Fortin, J., & Schubnel, A. (2024). Pressure dependence of permeability in cracked rocks: Experimental evidence of non-linear pore-pressure gradients from local measurements. *Geophysical Research Letters*, *51*(15). https://doi.org/10.1029/2024GL109308

Lissa, S., Barbosa, N. D., & Quintal, B. (2021). Fluid pressure diffusion in fractured media: The role played by the geometry of real fractures. *Journal of Geophysical Research: Solid Earth*, *126*(10), e2021JB022233. https://doi.org/10.1029/2021JB022233

Lissa, S., Barbosa, N. D., Rubino, J. G., & Quintal, B. (2019). Seismic attenuation and dispersion in poroelastic media with fractures of variable aperture distributions. *Solid Earth*, *10*(4), 1321–1336. https://doi.org/10.5194/se-10-1321-2019

Masson, Y. J., & Pride, S. R. (2014). On the correlation between material structure and seismic attenuation anisotropy in porous media. *Journal of Geophysical Research: Solid Earth*, *119*(4), 2848–2870. https://doi.org/10.1002/2013JB010798

Möllhoff, M., Bean, C. J., & Meredith, P. G. (2010). Rock fracture compliance derived trom time delays of elastic waves. *Geophysical Prospecting*, *58*, 1111–1121. https://doi.org/10.1111/j.1365-2478.2010.00887.x

Nakagawa, S. (2013). Low-frequency (<100Hz) dynamic fracture compliance measurement in the laboratory. In *47th US rock mechanics/geomechanics symposium* (pp. 13–343). ARMA.

O'Connell, R. J., & Budiansky, B. (1978). Measures of dissipation in viscoelastic media. *Geophysical Research Letters*, *5*(1), 5–8. https://doi.org/10.1029/gl005i001p00005

Passelègue, F. X., Almakari, M., Dublanchet, P., Barras, F., Fortin, J., & Violay, M. (2020). Initial effective stress controls the nature of earthquakes. *Nature Communications*, *11*(1), 5132. https://doi.org/10.1038/s41467-020-18937-0

Pimienta, L., Borgomano, J. V. M., Fortin, J., & Guéguen, Y. (2016). Modelling the drained/undrained transition: Effect of the measuring method and the boundary conditions. *Geophysical Prospecting*, *64*(4), 1098–1111. https://doi.org/10.1111/1365-2478.12390

Pini, R., & Benson, S. M. (2017). Capillary pressure heterogeneity and hysteresis for the supercritical CO2/water system in a sandstone. *Advances in Water Resources*, *108*, 277–292. https://doi.org/10.1016/j.advwatres.2017.08.011

Pride, S. R., & Berryman, J. G. (2003). Linear dynamics of double-porosity dual-permeability materials. I. Governing equations and acoustic attenuation. *Physical Review E*, *68*(3), 036603. https://doi.org/10.1103/physreve.68.036603

Pyrak-Nolte, L. J., Myer, L. R., & Cook, N. G. W. (1990). Transmission of seismic waves across single natural fractures. *Journal of Geophysical Research*, *95*(B6), 8617–8638. https://doi.org/10.1029/jb095ib06p08617

Quintal, B., Jänicke, R., Rubino, J. G., Steeb, H., & Holliger, K. (2014). Sensitivity of S-wave attenuation to the connectivity of fractures in fluid-saturated rocks. *Geophysics*, *79*(5), WB15–WB24. https://doi.org/10.1190/geo2013-0409.1

Quintal, B., Steeb, H., Frehner, M., & Schmalholz, S. M. (2011). Quasi-static finite element modeling of seismic attenuation and dispersion due to wave-induced fluid flow in poroelastic media. *Journal of Geophysical Research*, *116*(B1), B01201. https://doi.org/10.1029/2010JB007475

Rivet, D., De Barros, L., Guglielmi, Y., Cappa, F., Castilla, R., & Henry, P. (2016). Seismic velocity changes associated with aseismic deformations of a fault stimulated by fluid injection. *Geophysical Research Letters*, *43*(18), 9563–9572. https://doi.org/10.1002/2016GL070410

Rubino, J. G., Guarracino, L., Müller, T. M., & Holliger, K. (2013). Do seismic waves sense fracture connectivity? *Geophysical Research Letters*, *40*(4), 692–696. https://doi.org/10.1002/grl.50127

Rudnicki, J. W., & Zhan, Y. (2020). Effect of pressure rate on rate and state frictional slip. *Geophysical Research Letters*, *47*(21), e2020GL089426. https://doi.org/10.1029/2020GL089426

Schoenberg, M. (1980). Elastic wave behavior across linear slip interfaces. *Journal of the Acoustical Society of America*, *68*(5), 1516–1521. https://doi.org/10.1121/1.385077

Skempton, A. W. (1954). The pore-pressure coefficients A and B. *Géotechnique*, *4*, 143–147. https://doi.org/10.1680/geot.1954.4.4.143

Subramaniyan, S., Quintal, B., Tisato, N., Saenger, E. H., & Madonna, C. (2014). An overview of laboratory apparatuses to measure seismic attenuation in reservoir rocks. *Geophysical Prospecting*, *62*(6), 1211–1223. https://doi.org/10.1111/1365-2478.12171

Tisato, N., & Quintal, B. (2013). Measurements of seismic attenuation and transient fluid pressure in partially saturated berea sandstone: Evidence of fluid flow on the mesoscopic scale. *Geophysical Journal International*, *195*(1), 342–351. https://doi.org/10.1093/gji/ggt259

Viswanathan, H. S., Ajo-Franklin, J., Birkholzer, J. T., Carey, J. W., Guglielmi, Y., Hyman, J. D., et al. (2022). From fluid flow to coupled processes in fractured rock: Recent advances and new frontiers. *Reviews of Geophysics*, *60*(1), e2021RG000744. https://doi.org/10.1029/2021RG000744

Vo-Thanh, D. (1990). Effects of fluid viscosity on shear-wave attenuation in saturated sandstones. *Geophysics*, *55*(6), 712–722. https://doi.org/10.1190/1.1442883

Winkler, K., Nur, A., & Gladwin, M. (1979). Friction and seismic attenuation in rocks. *Nature*, *277*(5697), 528–531. https://doi.org/10.1038/277528a0

## References From the Supporting Information

Biot, M. A., & Willis, D. G. (1957). The elastic coefficients of the theory of consolidation. *Journal of Applied Mechanics*, *24*(4), 594–601. https://doi.org/10.1115/1.4011606